

Anomalous Fermi level behavior
in GaMnAs at the onset of ferromagnetism

Iriya Muneta^{*}, Hiroshi Terada, Shinobu Ohya, and Masaaki Tanaka[†]

Department of Electrical Engineering and Information Systems,

The University of Tokyo, 7-3-1 Hongo, Bunkyo-ku, Tokyo 113-8656, Japan

Abstract

We present the first systematic study of the resonant tunneling spectroscopy on a series of ferromagnetic-semiconductor $\text{Ga}_{1-x}\text{Mn}_x\text{As}$ with the Mn content x from ~ 0.01 to 3.2%. The Fermi level of $\text{Ga}_{1-x}\text{Mn}_x\text{As}$ exists in the band gap in the whole x region. The Fermi level is closest to the valence band (VB) at $x=1.0\%$ corresponding to the onset of ferromagnetism near the metal-insulator transition (MIT), but it moves away from the VB with increasing or decreasing x from 1.0%. This anomalous behavior of the Fermi level indicates that the ferromagnetism and MIT emerge in the Mn-derived impurity band.

PACS numbers: 85.75.Mm, 72.25.Dc, 73.40.Gk, 75.50.Pp

^{*} muneta@cryst.t.u-tokyo.ac.jp

[†] masaaki@ee.t.u-tokyo.ac.jp

The origin of the ferromagnetism and the metal-insulator transition (MIT) has been a long-debated issue in the prototype ferromagnetic semiconductor GaMnAs [1-4]. Previously, the valence band (VB) conduction picture has been widely accepted in this material [5], where the MIT of GaMnAs was understood by the Fermi level crossing over the VB [2,6] similarly to *p*-type GaAs doped with non-magnetic acceptors such as Be or Zn. The ferromagnetism in GaMnAs has been thought to be induced by the VB holes interacting with the localized *d* electrons of the Mn atoms [5,7]. However, recently, many experiments have shown the strong evidence that the Fermi level exists in the impurity band (IB) in the band gap [4,8-21], which requires reconsideration on the above scenario. Therefore, to clarify the origin of the ferromagnetism and MIT in GaMnAs, it is essential to precisely investigate the Fermi level position and the VB structure of GaMnAs in the low Mn content region including the onset of ferromagnetism and MIT.

Resonant tunneling spectroscopy is a powerful method to investigate the VB structure and the Fermi level position in GaMnAs with a precision of several meV. The advantage of this method is that we can detect the energy bands only with the same wave-function symmetry as that of the p-wave functions of the VB holes. Also, it is sensitive to the effective mass of the energy bands. Furthermore, by carefully analyzing the quantum-well (QW) thickness dependence of the resonant levels, we can avoid the unwanted effects induced at the surface, which prevent the precise

determination of the VB or the Fermi level position [22,3]. Recently, from the resonant tunneling experiments in the double-barrier (DB) QW heterostructures [14,15] and the single-barrier structures with an ultra-thin surface GaMnAs layer [16], it was shown that the Fermi level exists in the band gap in $\text{Ga}_{1-x}\text{Mn}_x\text{As}$ with the Mn content x higher than $\sim 5\%$. In this Letter, we carefully analyze the VB structure and the Fermi level position in a series of $\text{Ga}_{1-x}\text{Mn}_x\text{As}$ from the unexplored insulating region ($x \sim 0.01\%$) to the metallic region ($x = 3.2\%$). We find that the VB structure is not largely affected by the Mn doping and that the Fermi level never crosses over the VB near the MIT: The Fermi level becomes closest to the VB at $x = 1.0\%$ at the onset of the ferromagnetism, but it moves away from the VB with increasing or decreasing x from 1.0% . This anomalous behavior of the Fermi level is completely different from that of GaAs doped with other shallow acceptors.

Figure 1(a) shows the schematic device structures investigated in this study. We grew DB-QW heterostructures composed of (from the top to the bottom) $\text{Ga}_{0.94}\text{Mn}_{0.06}\text{As}$ (20 nm) / AlAs (6 nm) / $\text{Ga}_{1-x}\text{Mn}_x\text{As}$ QW (d nm) / AlAs (6 nm) / GaAs:Be (100 nm, Be concentration: $1 \times 10^{18} \text{ cm}^{-3}$) by low-temperature molecular-beam epitaxy (MBE). Table I shows the characteristics of the GaMnAs QW samples examined in this study. The Mn content x of sample D-H was determined by the x-ray diffraction measurements for 100 nm-thick reference GaMnAs samples grown in the same condition as that for the GaMnAs QW in each DB-QW sample. x of sample A-C was estimated from an

Arrhenius plot of the Mn flux vs. the K-cell temperature obtained from the flux data of sample D-H. In this study, x was varied from $\sim 0.01\%$ to 3.2% . In this Mn content range, with increasing x , GaMnAs changes from insulating paramagnetic to insulating ferromagnetic at $x \sim 1\%$. At $\sim 2\%$, it starts to show metallic behavior, in which the resistivity decreases with decreasing temperature T at $T < T_C$ (Curie temperature). The T_C values of the $\text{Ga}_{1-x}\text{Mn}_x\text{As}$ QW in sample D-H were obtained from the temperature dependence of tunneling magnetoresistance (TMR) observed in these devices. As shown in Table I, the $\text{Ga}_{1-x}\text{Mn}_x\text{As}$ QW with $x = 1 - 3\%$ has lower T_C than that of the surface $\text{Ga}_{0.94}\text{Mn}_{0.06}\text{As}$ (60 - 70 K) due to the low x in the QWs. To obtain the resonant tunneling diodes with various GaMnAs QW thickness d on a same wafer, we linearly moved a shutter in front of the substrate while growing the $\text{Ga}_{1-x}\text{Mn}_x\text{As}$ QW, in which d was varied from 10 nm to 16 nm within the wafer of $15 \times 10 \text{ mm}^2$ [23]. The values of d were estimated from the speed of the shutter. Although simpler structures (GaMnAs / AlAs / GaAs:Be single-barrier heterostructures) were used in Ref. 16, they are not applicable for this study due to the low Mn contents $< \sim 2\%$ in the GaMnAs QW that we are using here. The low Mn contents in the surface GaMnAs induce a large depletion thickness at the surface, making a electrical contact to the GaMnAs layer very difficult. Thus, the DB-QW structures are the best structure for our current purpose. The details about the preparation of the samples are described in the supplemental material [24].

Figure 1(b) shows the schematic VB profiles of the DB-QW devices shown in Fig. 1(a). The black solid and red dash-dotted lines indicate the VB top and Fermi level, respectively. The blue and orange lines are the resonant levels of the heavy hole (HH) and light hole (LH), respectively. Here, the small exchange splitting is neglected for simplicity. Figure 1(c) shows the schematic d dependence of the resonant levels. The resonant levels converge on the VB top energy E_V of the bulk GaMnAs with increasing d . Since the Fermi level corresponds to the zero bias condition, the Fermi level position can be determined by measuring the d dependence of the resonant levels. The bias polarity is defined by the voltage of the top GaMnAs electrode with respect to the substrate.

The solid curves in Fig. 2(a)-(c) show the d dependence of d^2I/dV^2-V in sample B, E, and H measured at 3.5 K in the negative bias region, respectively. The dashed curves labeled with HH n and LH n ($n = 1, 2, 3 \dots$) are resonant peaks assigned by the theoretical fitting mentioned later. Here, HH n and LH n are resonant tunneling through the n th level of the HH band and LH band in the Ga_{1-x}Mn_xAs QW, respectively. Clear oscillations due to the resonant tunneling are observed in all the d^2I/dV^2-V curves, and the resonant peak bias voltages become smaller with increasing d . In all the samples, the HH1 resonant level is clearly observed in the whole d region, which means that the Fermi level exists in the band gap. The d dependences of d^2I/dV^2-V in all the samples are shown in the supplemental material [24].

Figure 3 shows the VB diagram of the investigated DB-QW devices assumed in the following theoretical calculation of the resonant levels. The black solid and red dash-dotted lines are E_V and the Fermi level, respectively. The gray region is the band gap. For the quantum level calculation, we used the 4×4 Luttinger-Kohn $k \cdot p$ Hamiltonian [25] and transfer matrix method [26]. The VB offset between AlAs and GaMnAs was assumed to be 0.55 eV. We assumed that the in-plane wave vector k_{\parallel} is $\mathbf{0}$ during the tunneling, because holes are injected from the GaAs:Be electrode in the negative bias region and holes in the GaAs:Be electrode exist only around the Γ point. For simplicity, the small band bending was neglected.

Figure 4(a)-(c) show the color contour maps of the d^2I/dV^2 in sample B, E, and H as functions of $-V$ and d , respectively. Here, the color-coded intensities are extrapolated from the measured data at the d values corresponding to the white dots shown at the top of these figures. The black square and white triangle dots are calculated resonant peak bias voltages V_R of the HH and LH bands, respectively. E_F is the energy distance between E_V and the Fermi level. We determine the E_F values so that V_R and quantum level energy E_R have a linear relation $V_R = sE_R$. Also in the fitting, we slightly shifted the d value to d' in order to obtain the perfect fit. The value of d' used in the calculation was shown as the upper red ruler of the contour maps. The necessity of this shift of d is due to the difficulty in accurately controlling the relative positions between the substrate shutter and the sample wafer inside the MBE chamber.

We note that, however, the thickness difference between d and d' is only less than ~ 3 nm. The s value corresponds to the ratio of the total bias voltage to the voltage applied at the bottom AlAs barrier. The obtained s values are 1.8 - 2.4. Considering that s is 2 in ideal DB tunnel junctions [26] and that the s values obtained in the DB GaMnAs-QW heterostructures [14,15] were 2.4 - 3, the s values obtained in this study are quite reasonable. The color contour maps of the d^2I/dV^2 in all the samples are shown in the supplemental material [24].

In Fig. 5, the blue circles are the E_F values obtained in this study. The green squares are the ones reported in Ref. 16. The black pentagons are the thermal-activation energy E_a of the Mn acceptors in GaAs obtained by the magneto-transport measurements in Ref. 28. The pink curve is the calculated E_a values obtained from the equation $0.11[1-(x/1.0)^{1/3}]$ mentioned in Ref. 28. Here, we selected 1.0% as the intercept of x to fit the curve to the experimental data. The gray dash-dotted, dashed, and solid curves are the calculated E_F by the valence-band anti-crossing model (VBAC) [27] and the free-electron approximation. In the VBAC, the impurity level E_{imp} are assumed to be 0.1, 0.05, and 0.01 eV, respectively. Also, the anti-crossing coupling constant C_{Mn} is assumed to be and 0.18 eV. The free-electron approximation calculation for the Fermi level position in the IB is done by roughly assuming the hole concentration p to be $x/2$ and the effective mass to be $10m_e$ [11], where, m_e is the electron mass. Figure 5(b)-(d) show the VB and IB diagrams

derived from this study in the (b) insulating paramagnetic ($x < 1\%$), (c) insulating ferromagnetic ($x = 1-2\%$), and (d) metallic ferromagnetic ($x > 2\%$) regions, respectively. The black solid curves correspond to the VB. The blue dotted lines correspond to the upper and bottom edges of the IB. The blue region represents the IB region. The red dash-dotted lines correspond to the Fermi level. In the paramagnetic GaMnAs ($x < 1\%$), E_F decreases with increasing x , which is quantitatively consistent with the activation-energy-lowering effect observed in the magneto-transport measurements [28]. This behavior is the same as that observed in the insulating region of the non-magnetic acceptor-doped p -type GaAs [29]. The Fermi level behavior in the paramagnetic region is caused by the screening effect due to the heavy Mn doping, which makes the IB position close to the VB. On the other hand, E_F increases with increasing x in the ferromagnetic GaMnAs with $x > 1\%$, which means that the Fermi level moves away from the VB. This behavior is qualitatively explained by the VBAC model [the gray solid curve in Fig. 5(a)]. The quantitative discrepancy between the experimental and calculated Fermi level is probably because this calculation does not take into account the screening and many body effects. This Fermi level behavior in the ferromagnetic region means that the anti-crossing interaction overcomes the screening effect which is the main effect for determining the IB position in the paramagnetic region. Therefore, the IB becomes further away from the VB in the ferromagnetic region.

Figure 5 (a) shows that the Fermi level exists in the IB in the band gap in the whole

x region, which suggests that the ferromagnetism is strongly related to the IB. At the MIT border ($x \sim 2\%$), the Fermi level is still in the band gap, which suggests that the MIT occurs in the IB. This behavior of the Fermi level is completely different from that in the case of the heavily-doped p -type GaAs with the non-magnetic acceptors and contradicts the VB conduction picture, where the IB completely merges into the VB. The IB still exists in the metallic GaMnAs, which means that the impurity states still remain in the band gap. This is probably because the screening effect does not completely overcome the strong localization of the d -holes located within the screening length from the Mn atoms. At the onset of the ferromagnetism ($x \sim 1\%$), the x dependence of the Fermi level changes, which is thought to be induced by the change of the main effect for determining the IB position from the screening effect to the anti-crossing interaction. This must give a clue to understanding the mechanism of the ferromagnetism. We note that this anomalous behavior of the Fermi level is not directly related to the MIT because the MIT and the turning up of the Fermi level position occur at slightly different values of x (1.5 - 2% and $\sim 1\%$, respectively).

In summary, we fabricated the DB heterostructures containing a $\text{Ga}_{1-x}\text{Mn}_x\text{As}$ QW with the various x . From the resonant tunneling measurements in these structures, we found that the Fermi level exists in IB in the band gap in the whole range of x . When x is less than 1.0%, the Fermi level becomes close to the VB top with increasing x , which is induced by the screening effect. At $x=1.0\%$ around the emergence of the

ferromagnetism, the Fermi level becomes closest to the VB, where E_F is 4 meV. When x is larger than 1.0%, the Fermi level goes further away from the VB top with increasing x , which is qualitatively explained by the anti-crossing interaction. The x dependence of the Fermi level and the main effect for determining the IB position are different between the paramagnetic and ferromagnetic regions. Our results clearly show that the ferromagnetism and the MIT are strongly related to the formation of the Mn-derived IB.

This work was partly supported by Grant-in-Aids for Scientific Research including Specially Promoted Research, the Special Coordination Programs for Promoting Science and Technology, and FIRST Program of JSPS.

References

- [1] F. Matsukura, H. Ohno, A. Shen, and Y. Sugawara, *Phys. Rev. B* **57**, R2037 (1998).
- [2] T. Jungwirth, Jairo Sinova, A. H. MacDonald, B. L. Gallagher, V. Novák, K. W. Edmonds, A. W. Rushforth, R. P. Champion, C. T. Foxon, L. Eaves, E. Olejník, J. Mašek, S.-R. Eric Yang, J. Wunderlich, C. Gould, L. W. Molenkamp, T. Dietl, and H. Ohno, *Phys. Rev. B* **76**, 125206 (2007).
- [3] A. Richardella, P. Roushan, S. Mack, B. Zhou, D. A. Huse, D. D. Awschalom, A. Yazdani, *Science* **327**, 665 (2010).
- [4] B. C. Chapler, R. C. Myers, S. Mack, A. Frenzel, B. C. Pursley, K. S. Burch, E. J. Singley, A. M. Dattelbaum, N. Samarth, D. D. Awschalom, and D. N. Basov, *Phys. Rev. B* **84**, 081203(R) (2011).
- [5] T. Dietl, H. Ohno, F. Matsukura, J. Cibert, and D. Ferrand, *Science* **287**, 1019 (2000),
T. Dietl, H. Ohno, and F. Matsukura, *Phys. Rev. B* **63**, 195205 (2001).
- [6] T. Jungwirth, P. Horodyská, N. Tesařová, P. Němec, J. Šubrt, P. Malý, P. Kužel, C. Kadlec, J. Mašek, I. Němec, M. Orlita, V. Novák, K. Olejník, Z. Šobáň, P. Vašek, P. Svoboda, and Jairo Sinova, *Phys. Rev. Lett.* **105**, 227201 (2010).
- [7] J. Mašek, F. Máca, J. Kudrnovský, O. Makarovsky, L. Eaves, R. P. Champion, K. W. Edmonds, A. W. Rushforth, C. T. Foxon, B. L. Gallagher, V. Novák, Jairo Sinova, and T. Jungwirth, *Phys. Rev. Lett.* **105**, 227202 (2010).
- [8] K. Hirakawa, S. Katsumoto, T. Hayashi, Y. Hashimoto, and Y. Iye, *Phys. Rev. B* **65**, 193312 (2002).
- [9] V. F. Sapega, M. Moreno, M. Ramsteiner, L. Däweritz, and K. H. Ploog, *Phys. Rev. Lett.* **94**, 137401 (2005).

- [10] V. F. Sapega, N. I. Sablina, I. E. Panaiotti, N. S. Averkiev, and K. H. Ploog, *Phys. Rev. B* **80**, 041202(R) (2009).
- [11] K. S. Burch, D. B. Shrekenhamer, E. J. Singley, J. Stephens, B. L. Sheu, R. K. Kawakami, P. Schiffer, N. Samarth, D. D. Awschalom, and D. N. Basov, *Phys. Rev. Lett.* **97**, 087208 (2006).
- [12] K. Ando, H. Saito, K. C. Agarwal, M. C. Debnath, and V. Zayets, *Phys. Rev. Lett.* **100**, 067204 (2008).
- [13] M. Berciu, R. Chakarvorty, Y. Y. Zhou, M. T. Alam, K. Traudt, R. Jakiela, A. Barcz, T. Wojtowicz, X. Liu, J. K. Furdyna, and M. Dobrowolska, *Phys. Rev. Lett.* **102**, 247202 (2009).
- [14] S. Ohya, P. N. Hai, Y. Mizuno, and M. Tanaka, *Phys. Rev. B* **75**, 155328 (2007).
- [15] S. Ohya, I. Muneta, P. N. Hai, and M. Tanaka, *Phys. Rev. Lett.* **104**, 167204 (2010).
- [16] S. Ohya, K. Takata, and M. Tanaka, *Nat. Phys.* **7**, 342 (2011).
- [17] L. P. Rokhinson, Y. Lyanda-Geller, Z. Ge, S. Shen, X. Liu, M. Dobrowolska, and J. K. Furdyna, *Phys. Rev. B* **76**, 161201(R) (2007).
- [18] M. Yildirim, S. March, R. Mathew, A. Gamouras, X. Liu, M. Dobrowolska, J. K. Furdyna, and K. C. Hall, *Phys. Rev. B* **84**, 121202 (R) (2011).
- [19] K. Alberi, K. M. Yu, P. R. Stone, O. D. Dubon, W. Walukiewicz, T. Wojtowicz, X. Liu, and J. K. Furdyna, *Phys. Rev. B* **78**, 075201 (2008).
- [20] M. A. Mayer, P. R. Stone, N. Miller, H. M. Smith, O. D. Dubon, E. E. Haller, K. M. Yu, W. Walukiewicz, X. Liu, and J. K. Furdyna, *Phys. Rev. B* **81**, 045205 (2010).
- [21] M. Dobrowolska, K. Tivakornsasithorn, X. Liu, J. K. Furdyna, M. Berciu, K. M. Yu, and W. Walukiewicz, *Nat. Mater.* **11**, 444 (2012).

- [22] J. Okabayashi, A. Kimura, O. Rader, T. Mizokawa, A. Fujimori, T. Hayashi, and M. Tanaka, *Phys. Rev. B* **64**, 125304 (2001).
- [23] M. Tanaka and Y. Higo, *Phys. Rev. Lett.* **87**, 026602 (2001).
- [24] See Supplemental Material at [URL will be inserted by publisher] for the details about the sample preparation and the results in all the samples.
- [25] R. Wessel and M. Altarelli, *Phys. Rev. B* **39**, 12802 (1989).
- [26] R. Tsu and L. Esaki, *Appl. Phys. Lett.* **22**, 562 (1973).
- [27] K. Alberi, J. Wu, W. Walukiewicz, K. M. Yu, O. D. Dubon, S. P. Watkins, C. X. Wang, X. Liu, Y.-J. Cho, and J. Furdyna, *Phys. Rev. B* **75**, 045203 (2007).
- [28] J. S. Blakemore, Winfield J. Brown Jr, Merrill L. Stass, and Dustin A. Woodbury, *J. Appl. Phys.* **44**, 3352 (1973).
- [29] Dale. E. Hill, *J. Appl. Phys.* **41**, 1815 (1970).

TABLE I. Parameters and characteristics of the DB-QW samples investigated in this study. x is the Mn content of the $\text{Ga}_{1-x}\text{Mn}_x\text{As}$ QW. T_S is the growth temperature of the top AlAs barrier and the GaMnAs QW. d and T_C are the thickness and Curie temperature of the GaMnAs QW, respectively. E_F is the estimated energy distance between the Fermi level and the VB top at the Γ point in the GaMnAs QW.

Sample.	x (%)	T_S ($^{\circ}\text{C}$)	d (nm)	T_C (K)	E_F (meV)
Sample A	~ 0.01	400	10 - 16	paramagnetic	50
Sample B	~ 0.1	350	10 - 16	paramagnetic	30
Sample C	~ 0.3	330	10 - 16	paramagnetic	38
Sample D	1.0	265	10 - 16	25	4
Sample E	1.2	260	10 - 16	30	6
Sample F	1.6	250	10 - 16	40	10
Sample G	2.3	240	10 - 16	45	17
Sample H	3.2	230	10 - 16	60	25

Figure Captions

FIG. 1 (Color) (a) Schematic device structures investigated in this study. d_1 , d_2 , and d_3 are the GaMnAs QW thickness. (b) VB lineups of AlAs / GaMnAs QW / AlAs when the QW thickness is d_1 , d_2 , and d_3 . The black solid and red dash-dotted lines correspond to the VB top and Fermi level. The blue and orange lines correspond to the quantum levels in heavy and light hole bands, respectively. (c) d dependence of the quantum levels, where the blue and orange curves correspond to the heavy and light hole bands, respectively.

FIG. 2 (Color) (a)-(c) The black solid curves are the d^2I/dV^2 - V characteristics as a function of d in the DB-QW devices of (a) sample B, (b) sample E, and (c) sample H, respectively. The measurement temperature is 3.5 K. The dashed curves are the traces of the quantum levels. Here, HHn and LHn ($n: 1,2,3\dots$) represent resonant tunneling through the n th level of the HH and LH bands in GaMnAs QWs, respectively. Colors in these graphs express the d^2I/dV^2 intensity extrapolated from the measured data.

FIG. 3 (Color) VB diagram of the DB-QW devices used in the theoretical calculation. The black solid and red dash-dotted lines are E_V and the Fermi level, respectively. The gray region is the band gap.

FIG. 4 (Color) (a)-(c) The comparison between the calculated resonant levels and the experimentally obtained d^2I/dV^2 data of (a) sample B, (b) sample E, and (c) sample H as functions of $-V$ and d . The d^2I/dV^2 intensity is expressed by color. Here, these color intensities are extrapolated from the measured data with d corresponding to the white dots shown at the top of these figures. The connected black and white dots are the calculated resonant peak bias voltages V_R of the HH and LH bands, respectively. E_F , s , and d' are defined in the main text.

FIG. 5 (Color) (a) The blue circles and green squares are the E_F values obtained in this study and in Ref. 16, respectively. The black pentagons are the E_a values reported in Ref. 28. The pink curve is the calculated E_a . The gray dash-dotted, dashed, and solid curves are the calculated E_F with respect to E_V by the VBAC model [27] and the free-electron approximation. In the VBAC, E_{imp} are assumed to be 0.1, 0.05, and 0.01 eV, respectively. The red dashed curve connects the E_F values in $x > 1\%$. (b)-(d) The

VB and IB diagrams of GaMnAs derived from this study in the (b) insulating paramagnetic ($x < 1\%$), (c) insulating ferromagnetic ($x = 1-2\%$), and (d) metallic ferromagnetic ($x > 2\%$) regions. The black solid curves are the VB. The blue dotted lines are the upper and bottom edges of the IB. The blue region represents the IB region. The red dash-dotted lines are the Fermi level.

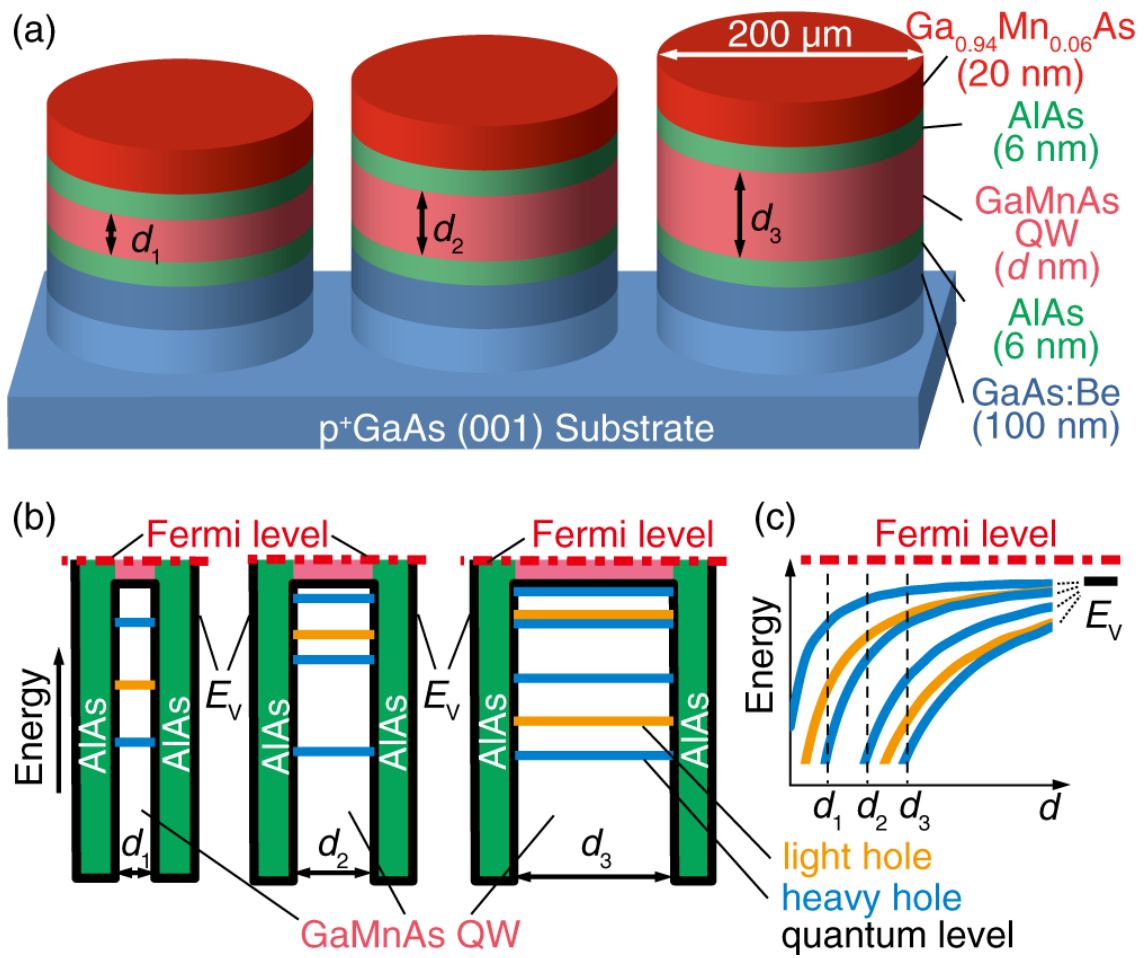


Figure 1 I. Muneta *et al.*

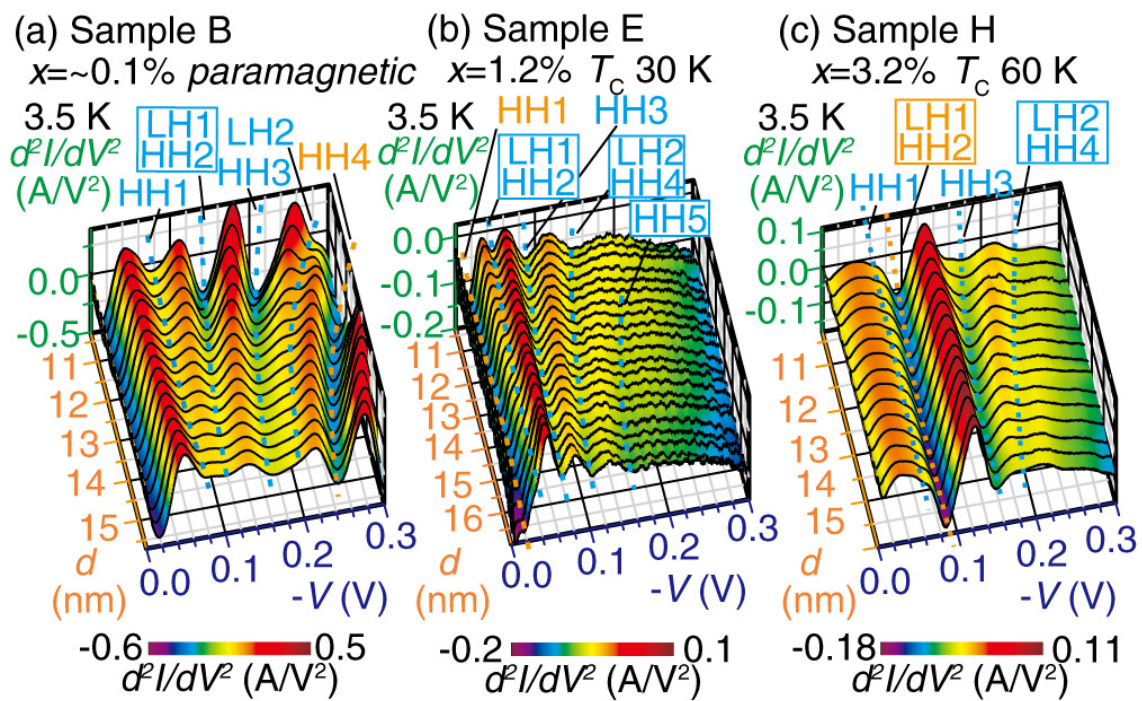


Figure 2 I. Muneta *et al.*

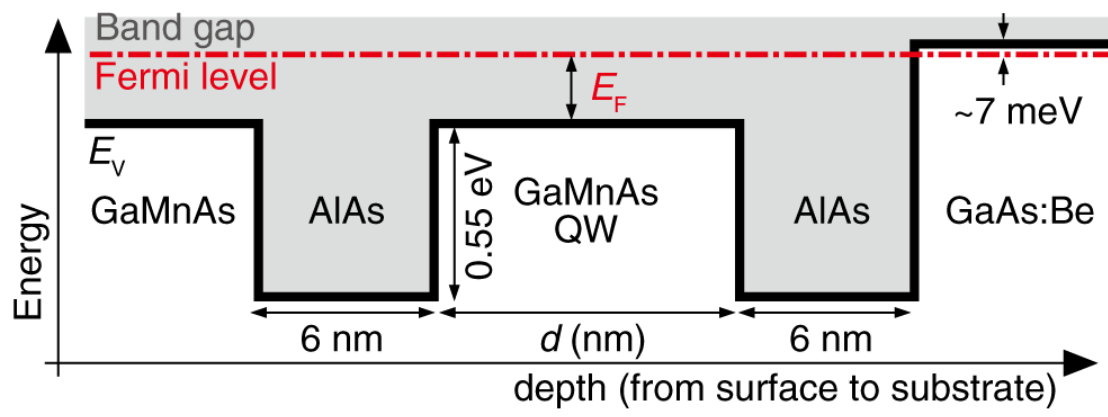


Figure 3 I. Muneta *et al.*

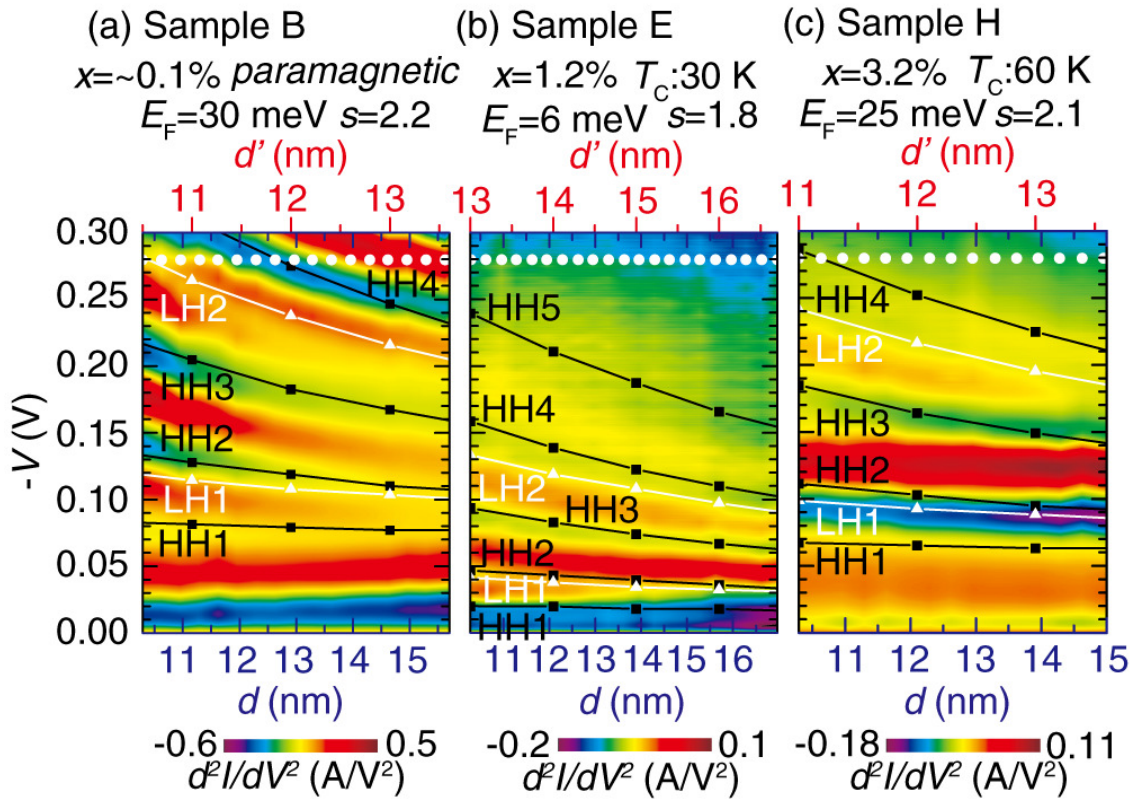


Figure 4 I. Muneta *et al.*

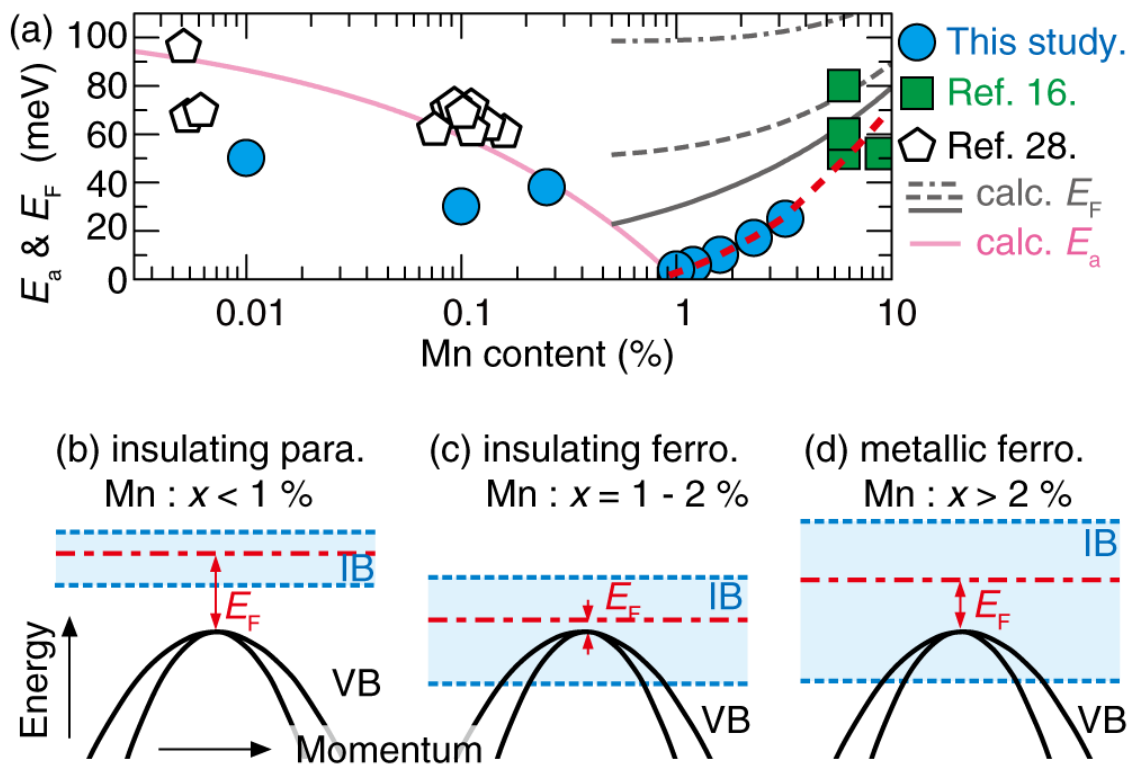


Figure 5 I. Muneta *et al.*